Analysis of globally connected active rotators with excitatory and inhibitory connections using the Fokker-Planck equation

Takashi Kanamaru and Masatoshi Sekine

Department of Electrical and Electronic Engineering, Faculty of Technology,

Tokyo Univ. of Agriculture and Technology, Tokyo 184-8588, Japan

(Dated: March 25, 2003)

Abstract

The globally connected active rotators with excitatory and inhibitory connections are analyzed using the nonlinear Fokker-Planck equation. The bifurcation diagram of the system is obtained numerically, and both periodic solutions and chaotic solutions are found. By observing the interspike interval, the coefficient of variance, and the correlation coefficient of the system, the relationship of our model to the biological data is discussed.

Physical Review E, vol.67 (2003) 031916.

PACS numbers: 87.10.+e, 05.45.−a, 84.35.+i, 07.05.Mh

I. INTRODUCTION

Recently, in the analyses of the experimental data obtained from the brain, the pulse trains from a single neuron and the correlations in the neuronal ensembles with various sizes have attracted considerable attentions, and their roles in information processing are discussed by numerous authors [1–5].

In Refs. [1–4], the apparently stochastic pulse trains from single neurons in the cortex are investigated, and the importance of the precise timing of each firing is examined. The role of a single pulse in the brain function is still controversial, but some experimental and theoretical researches have shown that the timing of the firings of single neurons is reliable and it can be a candidate for the carrier of the information in the brain [6–8].

On the other hand, the neuronal networks in the visual cortex and the hippocampus often show oscillatory behaviors, which imply that the neurons in the network emit the spikes synchronously (for reviews, see Ref. [5]). It is suggested that such synchronized oscillations contribute to the information processing, *e.g.*, the bindings of the visual informations in the visual cortex and the control of the synaptic plasticity in the hippocampus.

These experimental researches suggest that the theoretical analyses of the pulse neural networks are of importance to understand the brain function from the neuronal level [9].

To analyze the stochastic system governed by a Langevin equation, the Fokker-Planck equation is often used to describe the dynamics of the probability density of the system [10], and it is also applicable to the pulse neural networks. In Ref. [11], sparsely connected leaky integrate-and-fire models are analyzed by the Fokker-Planck equation. Under the condition of the sparse connection, the network are reduced to a single element with an input from the network, and its self-consistent Fokker-Planck equation is numerically analyzed. In Ref. [12], a layer network of leaky integrate-and-fire models is treated, and the formation of the synfire-chain is analyzed by the Fokker-Planck equation.

In the present paper, a globally connected pulse neural network with excitatory and inhibitory connections is analyzed using the Fokker-Planck equations. The neuron is modeled by the active rotator, and the connection imitates the synaptic connection in the brain. By virtue of the global connecting, a set of Fokker-Planck equations with nonlinear terms [13] can be introduced, thus the probability density of the whole network can be treated directly.

In Sec. II, the definition of our model is given and its Fokker-Planck equations are

introduced. In Sec. III, the Fokker-Planck equations are analyzed numerically, and the bifurcation diagram is obtained. The periodic solutions and the chaotic solutions are found in some parameter range. In Sec. IV, the chaotic solutions found in Sec. III are analyzed with the Poincaré section and the largest Lyapunov exponent. In Sec. V, the pulse trains of the model are analyzed using the interspike interval, the coefficients of variance, and the correlation coefficients. Conclusions and discussions are presented in the final section.

II. MODEL

Let us consider the globally connected active rotators with excitatory elements $\theta_E^{(i)}$ $(i = 1, 2, \cdots, N_E)$ and inhibitory elements $\theta_I^{(i)}$ $(i = 1, 2, \cdots, N_I)$ written as

$$\begin{aligned}
\dot{\theta_E^{(i)}} &= 1 - a\sin\theta_E^{(i)} + \xi_E^{(i)}(t) \\
&\quad + \frac{g_{EE}}{N_E}\sum_{j=1}^{N_E}(-\sin\theta_E^{(j)} + 1/a) \\
&\quad - \frac{g_{EI}}{N_I}\sum_{j=1}^{N_I}(-\sin\theta_I^{(j)} + 1/a), \qquad (1) \\
\dot{\theta_I^{(i)}} &= 1 - a\sin\theta_I^{(i)} + \xi_I^{(i)}(t) \\
&\quad + \frac{g_{IE}}{N_E}\sum_{j=1}^{N_E}(-\sin\theta_E^{(j)} + 1/a) \\
&\quad - \frac{g_{II}}{N_I}\sum_{j=1}^{N_I}(-\sin\theta_I^{(j)} + 1/a), \qquad (2) \\
\langle \xi_E^{(i)}(t)\xi_E^{(j)}(t')\rangle &= D\delta_{ij}\delta(t-t'), \qquad (3) \\
\langle \xi_I^{(i)}(t)\xi_I^{(j)}(t')\rangle &= D\delta_{ij}\delta(t-t'), \qquad (4) \\
\langle \xi_E^{(i)}(t)\xi_I^{(j)}(t')\rangle &= 0, \qquad (5)
\end{aligned}$$

where a is a system parameter and $\xi_E^{(i)}(t)$ and $\xi_I^{(i)}(t)$ are Gaussian white noises with the intensity D injected to the elements $\theta_E^{(i)}$ and $\theta_I^{(i)}$, respectively. For $a > 1$, the active rotator shows typical properties of an excitable system, namely, it has a stable equilibrium and $-\sin(\theta^{(i)}(t)) + 1/a$ shows a pulse-like waveform with an appropriate amount of disturbance. Although the active rotators are usually connected diffusively [14–17], the active rotators in our model are connected with the term $-\sin(\theta^{(i)}(t))+1/a$ to imitate the synaptic connections in the brain.

Let us consider the normalized number densities of the rotators having the phase θ_E and θ_I at time t written as

$$n_E(\theta_E, t) \equiv \frac{1}{N_E}\sum_{i=1}^{N_E}\delta(\theta_E^{(i)} - \theta_E), \tag{6}$$

$$n_I(\theta_I, t) \equiv \frac{1}{N_I}\sum_{i=1}^{N_I}\delta(\theta_I^{(i)} - \theta_I), \tag{7}$$

for the excitatory elements and inhibitory elements, respectively. With $n_E(\theta_E, t)$ and $n_I(\theta_I, t)$, Eqs. (1) and (2) are rewritten as

$$\begin{aligned}\dot{\theta_E^{(i)}} &= 1 - a\sin\theta_E^{(i)} + \xi_E^{(i)}(t) \\ &\quad + g_{EE}\int_0^{2\pi} d\phi_E(-\sin\phi_E + 1/a)n_E(\phi_E, t) \\ &\quad - g_{EI}\int_0^{2\pi} d\phi_I(-\sin\phi_I + 1/a)n_I(\phi_I, t),\end{aligned} \tag{8}$$

$$\begin{aligned}\dot{\theta_I^{(i)}} &= 1 - a\sin\theta_I^{(i)} + \xi_I^{(i)}(t) \\ &\quad + g_{IE}\int_0^{2\pi} d\phi_E(-\sin\phi_E + 1/a)n_E(\phi_E, t) \\ &\quad - g_{II}\int_0^{2\pi} d\phi_I(-\sin\phi_I + 1/a)n_I(\phi_I, t).\end{aligned} \tag{9}$$

In the limit of $N_E, N_I \to \infty$, $n_E(\theta_E, t)$ and $n_I(\theta_I, t)$ may be identified with the probability densities, and in this approximation $n_E(\theta_E, t)$ and $n_I(\theta_I, t)$ follow the nonlinear coupled Fokker-Planck equation [13] written as

$$\frac{\partial n_E}{\partial t} = -\frac{\partial}{\partial\theta_E}(A_E n_E) + \frac{D}{2}\frac{\partial^2 n_E}{\partial {\theta_E}^2}, \tag{10}$$

$$\frac{\partial n_I}{\partial t} = -\frac{\partial}{\partial\theta_I}(A_I n_I) + \frac{D}{2}\frac{\partial^2 n_I}{\partial {\theta_I}^2}, \tag{11}$$

$$\begin{aligned}A_E(\theta_E, t) &= 1 - a\sin\theta_E \\ &\quad + g_{EE}\int_0^{2\pi} d\phi_E(-\sin\phi_E + 1/a)n_E(\phi_E, t) \\ &\quad - g_{EI}\int_0^{2\pi} d\phi_I(-\sin\phi_I + 1/a)n_I(\phi_I, t),\end{aligned} \tag{12}$$

$$\begin{aligned}A_I(\theta_I, t) &= 1 - a\sin\theta_I \\ &\quad + g_{IE}\int_0^{2\pi} d\phi_E(-\sin\phi_E + 1/a)n_E(\phi_E, t) \\ &\quad - g_{II}\int_0^{2\pi} d\phi_I(-\sin\phi_I + 1/a)n_I(\phi_I, t).\end{aligned} \tag{13}$$

In the limit of $N_E, N_I \to \infty$, the dynamics of the elements can be followed by solving Eqs. (8) and (9) together with the nonlinear Fokker-Planck Eqs. (10) and (11) for a desired

number of elements, and we call it an infinite system. With the infinite system, we can investigate the interspike interval and the coefficient of variance of each element, and the correlation between two pulse trains from two elements in the system.

For simplicity, the strengths of connections are assumed to be $g_{EE} = g_{II} \equiv g_{int}$ and $g_{IE} = g_{EI} \equiv g_{ext}$, and the parameters are fixed as $a = 1.05$ and $g_{int} = 1.0$ in the following.

III. BIFURCATION ANALYSIS

Figures 1 (a), (b), and (c) show the numerical solutions of Eqs. (10) and (11) for (a) $D = 0.01$ and $g_{ext} = 0.2$, (b) $D = 0.02$ and $g_{ext} = 0.1$, and (c) $D = 0.03$ and $g_{ext} = 0.6$ with the uniform initial condition $n_E = n_I = 1/2\pi$, and Figs. 1 (d), (e), and (f) show the corresponding raster plots of the firing times of the finite system with $N_E = N_I = 1000$. The elements in the finite system are aligned so that the indices of the excitatory elements are in the range $0 \leq i < 1000$ and those of the inhibitory elements are in $1000 \leq i < 2000$. Note that the firing time of the i-th element is defined as the time when $-\sin(\theta^{(i)}(t)) + 1/a$ exceeds 1.5. For $D = 0.01$ and $g_{ext} = 0.2$ (Figs. 1 (a) and (d)), almost all the elements fluctuate around their equilibria and sometimes emit spikes, and n_E and n_I converge to the stationary densities. For $D = 0.02$ and $g_{ext} = 0.1$ (Figs. 1 (b) and (e)), the inhibitory elements fire randomly with low firing rates, and the excitatory elements fire periodically. The firings in each ensemble are asynchronous, thus the both densities converge to the stationary densities. For $D = 0.03$ and $g_{ext} = 0.6$ (Figs. 1 (c) and (f)), almost all the elements oscillate correlatively, and the densities also oscillate periodically. In the following, such firings are called synchronous firings.

In Fig. 2, a bifurcation diagram in the (D, g_{ext}) plane is shown. The open circles show the parameters where the numerically obtained n_E and n_I converge to the periodic solutions, and the solid and dotted lines are the Hopf bifurcation line and the saddle-node bifurcation line, respectively. Two saddle-node bifurcation lines intersect at a cusp bifurcation point, and a saddle-node bifurcation line, a Hopf bifurcation line and a saddle separatrix loop bifurcation line intersect at a Bogdanov-Takens bifurcation point [18, 19]. The Hopf and saddle-node bifurcation lines are obtained as follows. First, Eqs. (10) and (11) are transformed into a set of ordinary differential equations $\dot{\boldsymbol{x}} = \boldsymbol{f}(\boldsymbol{x})$ for the spatial Fourier coefficients of n_E and n_I. Next the stationary solution $\boldsymbol{x}_0$ which satisfies $\boldsymbol{f}(\boldsymbol{x}_0) = 0$ is numerically obtained, and

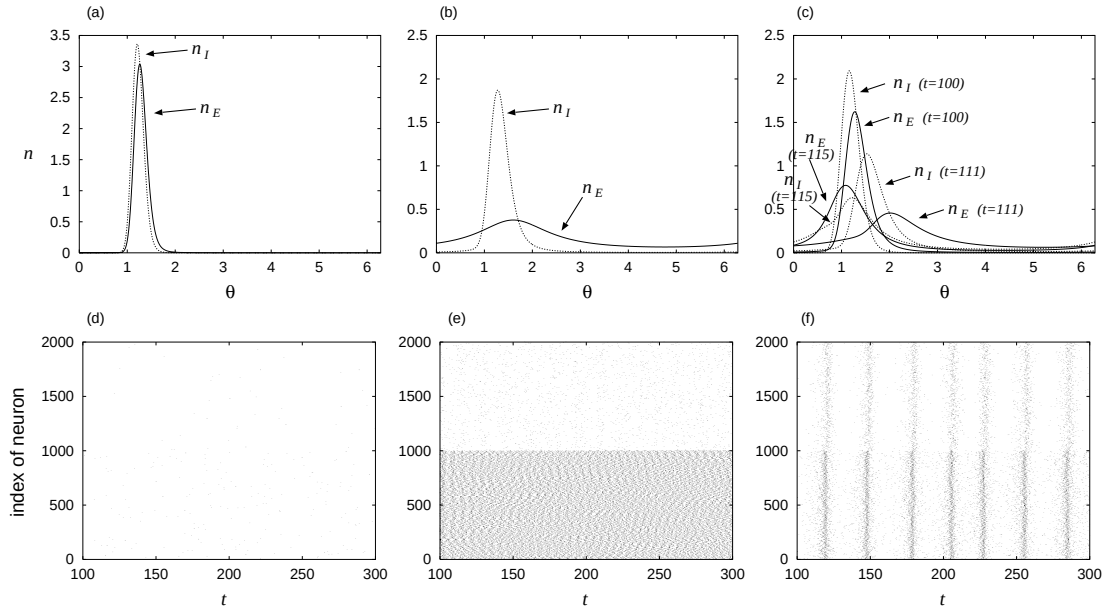

FIG. 1: The numerical solutions of the probability densities n_E and n_I for (a) $D = 0.01$ and $g_{ext} = 0.2$, (b) $D = 0.02$ and $g_{ext} = 0.1$, and (c) $D = 0.03$ and $g_{ext} = 0.6$. Figures (d), (e), and (f) are the corresponding raster plots of the firing times of the finite system with $N_E = N_I = 1000$. The elements in the finite system are aligned so that the excitatory elements are in the range $0 \leq i < 1000$ and inhibitory elements are in $1000 \leq i < 2000$.

the eigenvalues of the Jacobian matrix $D\boldsymbol{f}(\boldsymbol{x}_0)$ are analyzed numerically.

In the region around $(D, g_{ext}) \simeq (0.03, 0.37)$, a periodic solution is created by a bifurcation known as the double limit cycle bifurcation [19], namely, the simultaneous emergence of stable and unstable limit cycles. The double limit cycle bifurcation line is obtained from the long-time behavior of the solutions of Eqs.(10) and (11). Near the double limit cycle bifurcation line, the bifurcations to chaos also exist, and we treat them in Sec. IV. Moreover, when the double limit cycle bifurcation line approaches to the saddle-node bifurcation line, the bifurcations become more complex, namely, it seems that the chaotic orbit suddenly emerges when the system crosses the bifurcation line. The analysis of this bifurcation requires infinitely long computational times and the large numerical precision, thus we could not determine its mechanism.

To understand the bifurcation diagram in Fig. 2, let us define the probability fluxes [10]

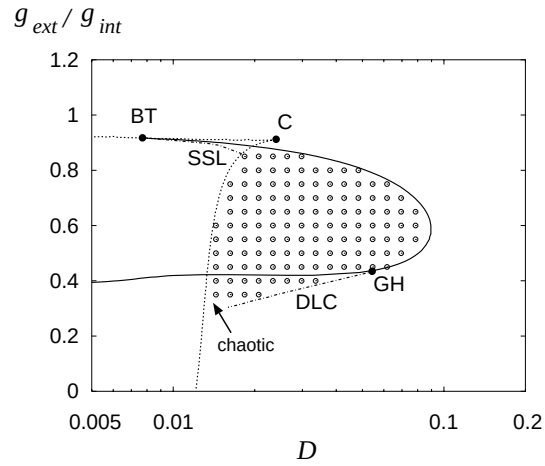

FIG. 2: A bifurcation diagram in the (D, g_{ext}) plane. The open circles show the parameters where the numerically obtained n_E and n_I converge to the periodic solutions, and the solid and dotted lines denote the Hopf bifurcation line and the saddle-node bifurcation line, respectively. The dash-dotted lines denote the global bifurcations of the saddle separatrix loop bifurcation and the double limit cycle bifurcation. The meanings of the abbreviations are as follows: C - cusp, BT - Bogdanov-Takens, SSL - saddle separatrix loop, GH - generalized Hopf, and DLC - double limit cycle.

for the excitatory and inhibitory ensembles as

$$J_E(\theta_E, t) = A_E n_E - \frac{D}{2}\frac{\partial n_E}{\partial \theta_E}, \tag{14}$$

$$J_I(\theta_I, t) = A_I n_I - \frac{D}{2}\frac{\partial n_I}{\partial \theta_I}, \tag{15}$$

and the fluxes at $\theta_E = \theta_I = 3/2\pi$ are observed in the following. Note that a stationary solution and a periodic solution of n_E and n_I are projected as a stationary point and a limit cycle onto the (J_E, J_I) plane, respectively.

In Fig. 3, a bifurcation diagram in the (D, g_{ext}) plane with schematic diagrams of the solutions in the (J_E, J_I) plane is shown. Typically, there exist stationary points S_0 with $(J_E, J_I) \sim (0, 0)$ and S_1 with $J_E > J_I > 0$, and a limit cycle emerges when S_0 disappears by the saddle-node on limit cycle bifurcation or when S_1 loses its stability by the Hopf bifurcation. Note that the stationary densities in Figs. 1 (a) and (b) correspond to S_0 and S_1, respectively, and the temporally oscillating densities in Fig. 1 (c) correspond to the limit cycle. A detailed schematic bifurcation diagrams are shown in Figs. 4 (a) and (b). Note

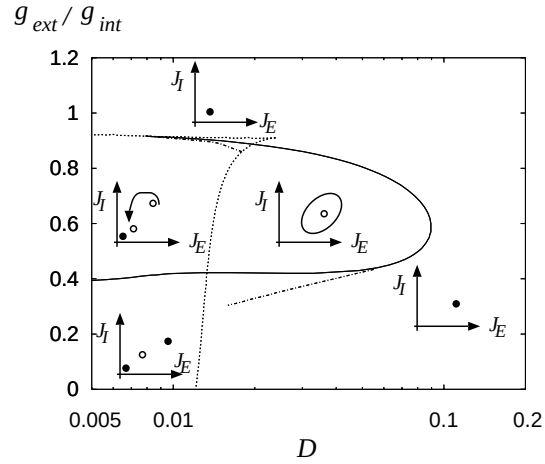

FIG. 3: A bifurcation diagram in the (D, g_{ext}) plane with schematic diagrams of the solutions in the (J_E, J_I) plane. The filled and open circles in the (J_E, J_I) plane denote the stable and unstable equilibrium points, respectively, and the solid closed curve denotes the stable limit cycle.

that a saddle separatrix loop bifurcation line is added to Fig. 4 (b) as a conjecture although we could not find it. From the trajectories shown in Fig. 4 (b), it is natural to assume the existence of such a bifurcation. Moreover, as stated above, when the double limit cycle bifurcation line in Fig. 4 (b) approaches to the saddle-node bifurcation line, the bifurcations become more complex. This bifurcation is no longer a double limit cycle bifurcation, but some bifurcation surely exists, thus we extend the double limit cycle bifurcation line with a dashed line in Fig. 4 (b). Similarly, the saddle-separatrix loop bifurcation may also become complex near the saddle-node bifurcation line, thus the SSL line is drawn with a dashed line near the SN line in Fig. 4 (b).

As shown above, the globally connected active rotators with excitatory and inhibitory connections show the oscillatory and synchronized behavior when the noise intensity D and the strength g_{ext} of connection between the ensembles are appropriately chosen. Such a oscillatory phenomenon is also observed in the system with two sigmoidal neurons one of which is excitatory and the other is inhibitory [19]. By regarding the change of threshold of the sigmoidal neuron as the change of the noise intensity D, and interpreting the output of the sigmoidal neuron as the spatial firing rate of the neuronal ensemble, the network with two sigmoidal neurons corresponds to our model. In other words, an oscillatory phenomenon of two sigmoidal neurons is derived from a pulse neural network with infinite numbers of

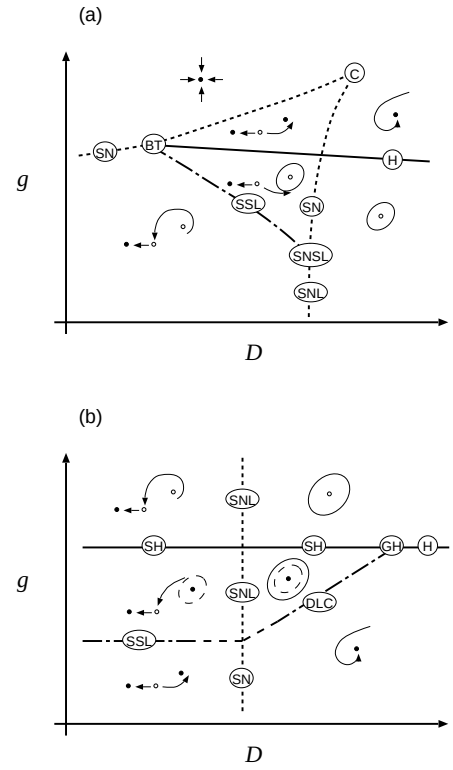

FIG. 4: A detailed schematic bifurcation diagrams around (a) the saddle separatrix loop and (b) the double limit cycle bifurcation. The solid and dotted lines denote the Hopf bifurcation line and the saddle-node bifurcation line, respectively. The dash-dotted lines denote the global bifurcations of the saddle separatrix loop bifurcation and the double limit cycle bifurcation. The saddle separatrix loop bifurcation line in Fig. (b) is added as a conjecture (see text for detail). The trajectories in the (J_E, J_I) plane are also illustrated. The filled and open circles in the trajectories denote the stable and unstable equilibrium points, respectively. And the solid and dashed closed curves denote the stable and unstable limit cycle, respectively. The meanings of the abbreviations are as follows: SN - saddle-node, H - Hopf, C - cusp, BT - Bogdanov-Takens, SSL - saddle separatrix loop, SNSL - saddle-node separatrix loop, SNL - saddle-node on limit cycle, GH - generalized Hopf, DLC - double limit cycle, and SH - subcritical Hopf.

excitatory and inhibitory neurons.

However, we are concerned with the importance of the pulses in the information processing, thus we analyze the network with the interspike interval, the coefficient of variance, and the correlation of the pulse trains in Sec. V.

IV. CHAOS ANALYSIS

As stated in Sec. III, the bifurcations to chaos exist near the double limit cycle bifurcation line. Let us consider the probability fluxes J_E and J_I at $\theta_E = \theta_I = 3/2\pi$. A time series of J_E for $D = 0.017$ and $g_{ext} = 0.32$ is shown in Fig. 5 (a), and it is observed that J_E oscillates aperiodically. The trajectory of this time series in the (J_E, J_I) plane is shown in Fig. 5 (b), and it seems to form a chaotic attractor.

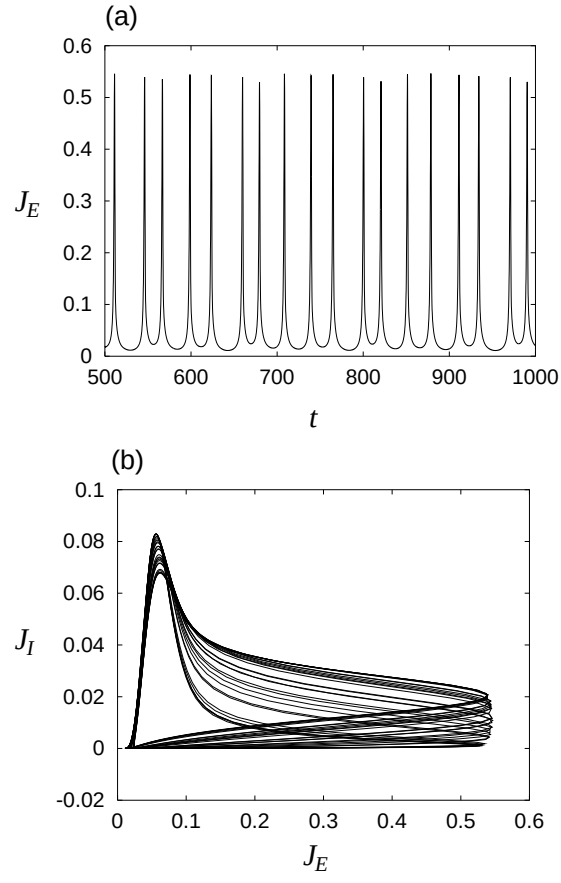

FIG. 5: (a) A time series of J_E and (b) its trajectory in the (J_E, J_I) plane for $D = 0.017$ and $g_{ext} = 0.32$.

Let us consider the Poincaré section at the line $J_E = 0.3$, and observe the points when the trajectory crosses this line in the positive direction. The position of the attractor on the Poincaré section against D for $g_{ext} = 0.32$ is shown in Fig. 6 (a). The range of D is chosen to cover the range where the periodic solution is stable, namely, the range between the saddle-node on limit cycle bifurcation at $D \simeq 0.013$ and the double limit cycle bifurcation

at $D \simeq 0.0185$. The period-doubling bifurcation and the transition to chaos are observed. Note that there exist periodic solutions whose periods are approximately multiples of the original limit cycle when chaos does not exists. To confirm that the observed dynamics is

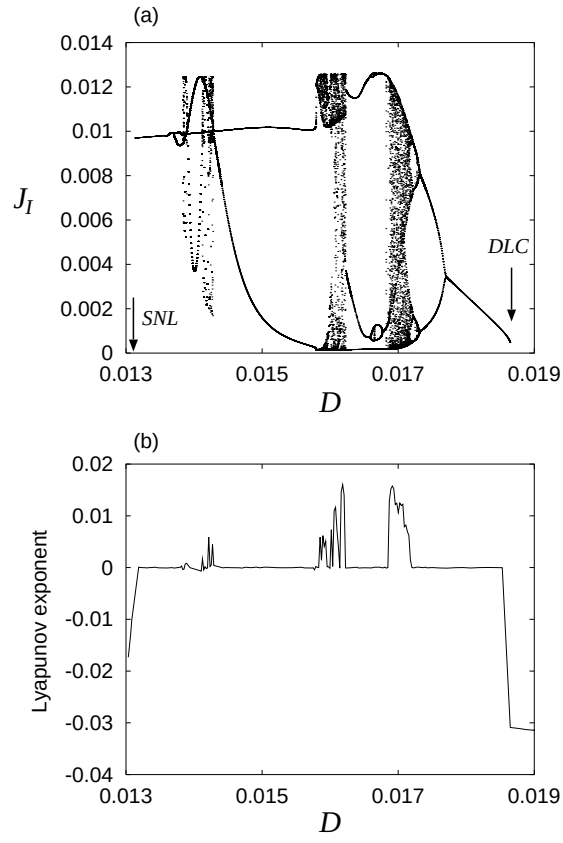

FIG. 6: (a) A bifurcation diagram for $g_{ext} = 0.32$. The points at which the trajectory crosses the line $J_E = 0.3$ in the positive direction are plotted. (b) The corresponding largest Lyapunov exponent.

actually chaotic, the largest Lyapunov exponent is calculated with a standard technique [20], namely, by calculating the expansion rate of two nearby trajectories each of which follows a set of ordinary differential equations $\dot{\boldsymbol{x}} = \boldsymbol{f}(\boldsymbol{x})$ for the spatial Fourier coefficients of Eqs. (10) and (11). In Fig. 6 (b), the corresponding largest Lyapunov exponent is shown. It is observed that it takes positive values when chaotic solutions exist, and takes zero when periodic solutions are stable.

V. PULSE ANALYSIS

In the previous sections, the Fokker-Planck equations (10) and (11) are numerically analyzed, and the dynamics of the excitatory and inhibitory ensembles is investigated. In this section, the infinite system described by Eqs. (8), (9), (10), and (11) is treated because the infinite system is useful for comparing our model with the experimental data of a single neuron. In this section, only the parameters where the system has time-varying solutions are treated.

First, let us define the interspike interval (ISI) as

$$T_k = t_{k+1} - t_k, \tag{16}$$

where t_k is the k-th firing of the element. With T_k, the coefficient of variance of the pulse train $\{t_k\}_k$ is defined as

$$C_V = \frac{\sqrt{\langle T_k^2 \rangle - \langle T_k \rangle^2}}{\langle T_k \rangle}, \tag{17}$$

where $\langle \cdot \rangle$ denotes the average over k. C_V takes large values for random pulse trains, and takes zero for periodic pulse trains. The mean interspike interval $T \equiv \langle T_k \rangle$ and C_V are used to investigate the properties of a single pulse train. In the following, the mean interspike intervals and the coefficients of variance of the excitatory and inhibitory elements are denoted as T_E, T_I, C_{VE}, and C_{VI}, respectively.

Next, let us define the correlation coefficient C between two pulse trains [21]. Usually, the correlation between two phase models is measured by the order parameter $\langle \cos(\theta_i - \theta_j) \rangle$, but it takes large values even when two rotators are fluctuating around their equilibria, thus it is not appropriate to measure the correlation between two pulse trains. To define C, the time under observation is divided into n bins of the width Δ, and the number of pulses in the i-th bin is denoted as X_i and Y_i for two pulse trains. Note that the width Δ is sufficiently small so that X_i and Y_i take the value 0 or 1. Then $X = \sum X_i$ and $Y = \sum Y_i$ are the numbers of pulses, and $Z = \sum X_i Y_i$ is the number of coincident pulses. The correlation coefficient C between two pulse trains is defined as

$$C = \frac{Z - (XY)/n}{\sqrt{X(1 - X/n)Y(1 - Y/n)}} \in [-1, 1]. \tag{18}$$

Note that C takes the value 1 for the identical pulse trains and takes the value 0 in the large n limit for two pulse trains without correlation. And C takes the value -1 when two pulse

trains have a negative correlation, namely, $X_i + Y_i = 1$ for $i = 0, 1, 2, \cdots$. In the following, the value $\Delta = 5$ is used.

Let us consider two infinite systems, each of which is governed by (8), (9), (10), and (11) with statistically independent noises. This system is composed of two excitatory and two inhibitory elements, and each element is statistically identical with the one in the original system with infinite numbers of elements. Thus the correlations between two elements in the infinite system reflect the correlation among the elements in the original finite system. In the following, the correlations between two excitatory elements and between two inhibitory elements are denoted as C_{EE} and C_{II}, respectively.

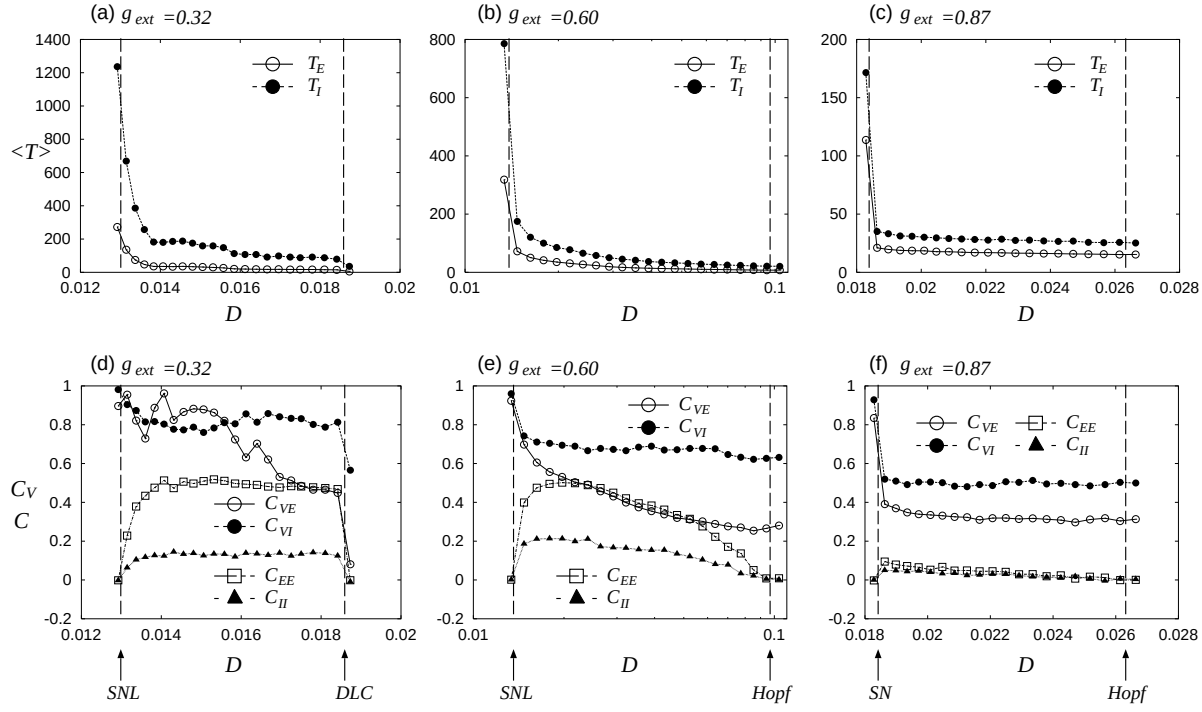

FIG. 7: The dependence of T on D for (a) $g_{ext} = 0.32$, (b) $g_{ext} = 0.60$, and (c) $g_{ext} = 0.87$, and the dependences of C_V and C on D for (d) $g_{ext} = 0.32$, (e) $g_{ext} = 0.60$, (f) $g_{ext} = 0.87$.

The dependences of T_E, T_I, C_{VE}, C_{VI}, C_{EE}, and C_{II} on the noise intensity D is shown in Fig. 7 for three values of g_{ext}.

For $g_{ext} = 0.32$, with the increase of D, a periodic solution emerges by the saddle-node on limit cycle (SNL) bifurcation, and it disappears by the double limit cycle (DLC) bifurcation after a series of bifurcations to chaos. For values of D close to SNL, each element spends a long time around its original equilibrium, thus T takes large values. And, reflecting the

existence of chaos and periodic solutions with n-cycles, C_V tends to take large values, but the excitatory ensemble has high correlations.

For $g_{ext} = 0.60$, with the increase of D, a periodic solution emerges with SNL and disappears by the Hopf bifurcation. For values of D close to SNL, both T and C_V take large values, and the ensemble of the excitatory elements has relatively high correlations. For values of D close to the Hopf bifurcation, T, C_V, and C take small values, thus all the elements oscillate asynchronously with a high frequency.

For $g_{ext} = 0.87$, with the increase of D, a stable stationary point disappears by the saddle-node bifurcation, then the system transits to the stable limit cycle (see Fig. 4 (a)), and a limit cycle disappears by the Hopf bifurcation. For all values of D, T, C_V, and C take small values, thus all the elements oscillate asynchronously with a high frequency.

Note that the inhibitory elements tend to take larger T and C_V, and smaller C than the excitatory elements in all the cases. It is because the inhibitory elements have small firing-rates and there exist the periods without firings as shown in Fig. 1 (f).

Following Brunel [11], let us classify the oscillations of excitatory elements based on three properties, namely, the frequency (fast or slow), the degree of synchronization (synchronous or asynchronous), and the randomness (regular or irregular). For example, the abbreviation FAR denotes the fast, asynchronous, and regular firings. With such a classification, the comparison between our results and the experimental data may become easier. The classification by Brunel is based only on the degree of synchronization and the randomness, thus our FAR firings correspond to Brunel's AR firings. Note that the bifurcation structure of our model differs from Brunel's one, and we consider only the parameters which yield time-varying solutions, thus the same abbreviation does not necessarily imply the similar firings. To compare the both firings, see Ref. [11].

A classification of the firings of excitatory elements in the (D, g_{ext}) plane is shown in Fig. 8. Typically, the FAR firing is observed near the Hopf bifurcation, and the SSI firing is observed near SNL. For the parameters which yield chaos, the randomness of the system is caused by both noise and chaos, and such firings are denoted as SSI*. Typical time series of J_E obtained from the Fokker-Planck equation and the firing times of the elements in the finite system for FAR, SSI, and SSI* firings are shown in Fig. 9. As stated above, SSI and SSI* firings have large C_V values because there are some noise-induced firings in the periods between two synchronous firings. Moreover, as shown in Fig.9 (e), the intervals of

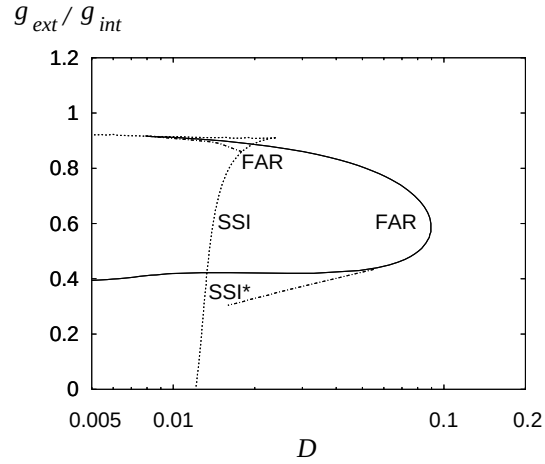

FIG. 8: A classification of the firings of excitatory elements in the (D, g_{ext}) plane.

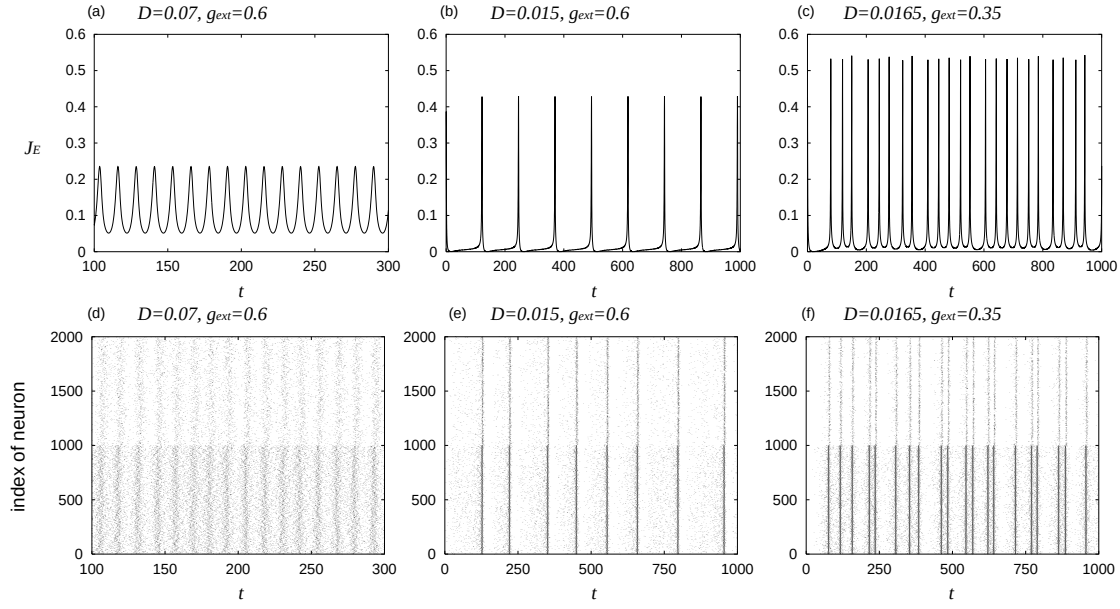

FIG. 9: Typical time series of (a), (d) FAR, (b), (e) SSI, and (c), (f) SSI* firings. Figures (a), (b), and (c) show J_E obtained from Fokker-Planck equation, and Figs. (d), (e), and (f) show the firing times of the finite system with $N_E = N_I = 1000$.

synchronous firings in SSI firings are not constant because of the finite-size effect.

To analyze SSI* firings, the detection of chaos is required, but it is difficult because noise hides chaos. In such a situation, the detection of the deterministic structure based on the normalized prediction error (NPE) may be useful [22, 23].

VI. CONCLUSIONS AND DISCUSSIONS

The globally connected active rotators with excitatory and inhibitory connections under noise are analyzed using the nonlinear Fokker-Planck equation, and their oscillatory phenomena are investigated numerically. Typically, the FAR (fast, asynchronous, and regular) oscillations are observed near the Hopf bifurcation line, and the SSI (slow, synchronous, and irregular) oscillations are observed near the saddle-node on limit cycle bifurcation line. Moreover, the SSI* oscillations where chaos and noise coexist are also observed.

In the cortex, the spike trains with high C_V, namely, the highly random spike trains are often observed experimentally, and their roles in information processing in the brain are discussed [1–4]. Our results show that the spike trains with high C_V do not necessarily imply that the network oscillates asynchronously, but there is a case where the elements in the network have some degree of correlations. Particularly, the SSI* oscillations have high C_V and high correlations (Figs. 7 (a) and (d)).

On the other hand, in the visual cortex and the hippocampus, various kinds of synchronous oscillations are observed, and their relations to the integration of the visual informations and the learning process of the memory are discussed [5]. Though the mechanism of the generations of such oscillations has not been fully understood, many researchers emphasize the importance of the inhibitory neurons based on both experimental and theoretical studies [24–27]. Especially, the experimental data in Ref. [27] implies that the network with excitatory and inhibitory neurons contributes to the 40-Hz oscillatory activity in the hippocampal CA3 area of rats and such a network might relate to our model.

Acknowledgments

The author (T.K.) is grateful to Professor Takehiko Horita for his careful reading of the manuscript. This research was partially supported by a Grant-in-Aid for Encouragement of Young Scientists (B) (No. 14780260) from the Ministry of Education, Culture, Sports, Science, and Technology, Japan.

[1] W. R. Softky and C. Koch, J. Neurosci. **13**, 334 (1993).

[2] M. N. Shadlen and W. T. Newsome, Curr. Opin. Neurobiol. **4**, 569 (1994).

[3] W. R. Softky, Curr. Opin. Neurobiol. **5**, 239 (1995).

[4] M. N. Shadlen and W. T. Newsome, Curr. Opin. Neurobiol. **5**, 248 (1995).

[5] C. M. Gray, J. Comput. Neurosci. **1**, 11 (1994).

[6] R. R. de Ruyter van Steveninck, G. D. Lewen, S. P. Strong, R. Koberle, and W. Bialek, Science **275**, 1805 (1997).

[7] M. J. Berry, D. K. Warland, and M. Meister, Proc. Nat. Acad. Sci. USA **94**, 5411 (1997).

[8] Z. F. Mainen and T. J. Sejnowski, Science **268**, 1503 (1995).

[9] *Pulsed Neural Networks*, edited by W. Maass and C. M. Bishop (The MIT Press, Chambridge, 1999).

[10] C. W. Gardiner, *Handbook of Stochastic Methods* (Springer-Verlag, Berlin, 1985).

[11] N. Brunel, J. Comput. Neurosci. **8**, 183 (2000).

[12] H. Câteau and T. Fukai, Neural Networks **14**, 675 (2001).

[13] Y. Kuramoto, *Chemical Oscillations, Waves, and Turbulence* (Springer, Berlin, 1984).

[14] S. Shinomoto and Y. Kuramoto, Prog. Theor. Phys. **75**, 1105 (1986).

[15] H. Sakaguchi, S. Shinomoto, and Y. Kuramoto, Prog. Theor. Phys. **79**, 600 (1988).

[16] C. Kurrer and K. Schulten, Phys. Rev. E **51**, 6213 (1995).

[17] S. Tanabe, T. Shimokawa, S. Sato, and K. Pakdaman, Phys. Rev. E **60**, 2182 (1999).

[18] J. Guckenheimer and P. Holmes, *Nonlinear Oscillations, Dynamical Systems, and Bifurcations of Vector Fields* (Springer, New York, 1983).

[19] F. C. Hoppensteadt and E. M. Izhikevich, *Weakly Connected Neural Networks* (Springer, New York, 1997).

[20] E. Ott, *Chaos in Dynamical Systems* (Cambridge University Press, New York, 1993).

[21] G. Palm, A. M. H. J. Aertsen, and G. L. Gerstein, Biol. Cybern. **59**, 1 (1988).

[22] T. Sauer, Phys. Rev. Lett. **72**, 3811 (1994).

[23] Y. Shinohara, T. Kanamaru, H. Suzuki, T. Horita, and K. Aihara, Phys. Rev. E **65**, 051906 (2002).

[24] R. D. Traub, R. Miles, and R. K. S. Wong, Science **243**, 1319 (1989).

[25] M. A. Whittington, R. D. Traub, and J. G. R. Jefferys, Nature **373**, 612 (1995).

[26] X-J. Wang and G. Buzsáki, J. Neurosci. **16**, 6402 (1996).

[27] A. Fisahn, F. G. Pike, E. H. Buhl, and O. Paulsen, Nature **394**, 186 (1998).